Frequency-selection mechanism in incompressible open-cavity flows via reflected instability waves

F. Tuerke,[1,2,3,*] D. Sciamarella,[4] L. R. Pastur,[3,4] F. Lusseyran,[3,4] and G. Artana[1,2]

[1]*Departamento de Ingeniería Mecánica, Universidad de Buenos Aires, Ciudad Autónoma de Buenos Aires, C1063ACV Argentina*

[2]*CONICET–Consejo Nacional de Investigaciones Científicas y Técnicas, C1083ACA Argentina*

[3]*Université Paris Sud 11, 91400 Orsay, France*

[4]*LIMSI-CNRS, 91400 Orsay, France*

(Received 31 July 2014; revised manuscript received 23 October 2014; published 8 January 2015)

We present an alternative perspective on nonharmonic mode coexistence, commonly found in the shear layer spectrum of open-cavity flows. Modes obtained by a local linear stability analysis of perturbations to a two-dimensional, incompressible, and inviscid sheared flow over a cavity of finite length and depth were conditioned by a so-called coincidence condition first proposed by Kulikowskii [J. Appl. Math. Mech. **30**, 180 (1966)] which takes into account instability wave reflection within the cavity. The analysis yields a set of discrete, nonharmonic frequencies, which compare well with experimental results [Phys. Fluids **20**, 114101 (2008); Exp. Fluids **50**, 905 (2010)].

DOI: 10.1103/PhysRevE.91.013005 PACS number(s): 47.20.Ft, 47.20.Cq

I. INTRODUCTION

Open-cavity flow, a canonical flow geometry of practical as well as academic interest in fluid mechanics, exhibits shear layer instabilities that have been subject to extensive, theoretical [1,2], and experimental [3,4,11,12] as well as numerical [5,6] studies over the course of the past decades. Resonant frequencies, commonly observed in open-cavity flows, were explained in terms of flow-acoustic feedback mechanisms [7] coupled with secondary hydrodynamic instabilities in the recirculation region of the cavity as well as three-dimensional instabilities [6]. Yet another mechanism was proposed by Villermaux and Hopfinger [8] to explain the low frequency content in the shear layer spectrum as a result of the recirculation region.

In the compressible subsonic regime, the well-known semiempirical Rossiter [7] formula, which was derived based on the assumption of acoustic feedback, describes the resonance frequencies observed in such flows reasonably well [9]. Interestingly, the nonharmonic modes were found experimentally also in the incompressible case by different groups [11,12]. Yamouni *et al.* [10] recently tried to link the compressible to the incompressible dynamics by means of a global linear stability analysis. His results, however, do not compare well with experimental data [11,12]. Hence the phenomenon still lacks a comprehensive explanation.

In the same decade as Rossiter presented his formula, Kulikowskii [13] derived a condition for linear stability analysis in a finite domain (LSAFD) that takes into account an amplified downstream traveling perturbation wave k_+ as well as an evanescent upstream traveling perturbation wave k_-. The waves are reflected at the downstream and upstream boundaries characterized by the reflection coefficients R_1 and R_2, respectively. In order for the perturbation to be self-sustaining, the amplitude of a perturbation wave at a given point in space must, after successive reflections, coincide with the amplitude of the original perturbation. Doaré and Langre [14] retrieved the same results as Kulikowskii, considering the complex Ginzburg-Landau amplitude equation in a finite domain together with a phase and energy closure principle first proposed by Gallaire and Chomaz [15]. Lindzen and Rosenthal [16] showed that Kelvin-Helmholtz instabilities result from wave overreflection in vertical direction with their energy extracted from the mean flow. Kulikowskii [17] himself continued research on this subject considering a two-dimensional domain, where waves can propagate and be reflected.

Open-cavity flow under the incompressible assumption is commonly described in terms of two physically different flow types: the recirculating flow inside the cavity and the shear layer flow above. The emitted frequencies observed experimentally are most likely the result of both the three-dimensional instabilities in the recirculation region and the shear layer instabilities [6]. None of the previous studies, however, consider the possibility (and consequences) of including the reflection of instability waves. In order to gain further insight into the nature of the mode coexistence in open-cavity flows, the present work analyzes the phenomenon through a local linear stability analysis (in the sense of Ref. [18]) together with the reflection of the instability waves from both cavity edges. The Kulikowskii condition is applied within the time asymptotic theory of spatiotemporal linear stability analysis, described in detail in Ref. [1] for plasma physics. The present work presents solutions of the Kulikowskii condition combined with a spatiotemporal linear stability analysis, thus obtaining a theoretical account for the nonharmonic mode coexistence commonly found in open-cavity flows. The results will be compared with six experiments of the $L/H = 2$ cavity geometry, published in Refs. [11] and [12].

The article is organized as follows. A short overview of the conventional spatiotemporal linear stability analysis is given in Sec. II. The physical argument of the Kulikowskii condition and the method developed to find solutions is presented in Sec. III. In Sec. IV the experiments with which the theory is compared are introduced, and thereafter the results of the LSAFD are presented. Conclusions are drawn in Sec. V.

*ftuerke@fi.uba.ar

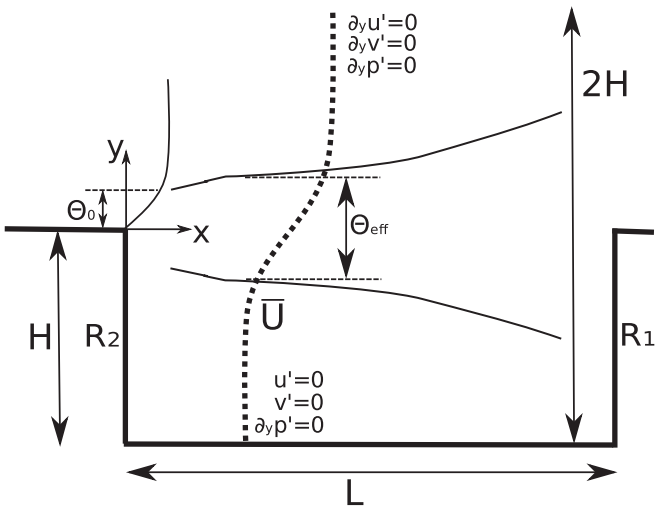

FIG. 1. Schematic view of cavity geometry with base flow $\overline{U}$, reflection coefficients R_1 and R_2, boundary conditions, inflow momentum thickness Θ_0, and effective momentum thickness Θ_{eff} used in the linear stability analysis and defined in Sec. IV A.

II. LINEAR STABILITY ANALYSIS

The flow is assumed to be steady, parallel, and unidirectional. The streamwise development of the base flow is therefore entirely neglected. The analysis of flow stability considers the two-dimensional, inviscid, and incompressible Euler equations given by

$$\partial_t \mathbf{u} + \mathbf{u}\cdot\nabla\mathbf{u} = -\nabla p, \tag{1}$$

$$\nabla\cdot\mathbf{u} = 0, \tag{2}$$

where $\mathbf{u} = (u,v)^T$. As in Huerre and Monkewitz [2] the flow variables $\mathbf{q}(x,y,t) = (u,v,p)^T$ and coordinates x,y are nondimensionalized using the average velocity $\tilde{U}$ and an effective momentum thickness Θ_{eff}, introduced in Sec. IV. The flow is decomposed into a steady laminar base flow $\overline{\mathbf{Q}}(y) = (\overline{U},\overline{V},\overline{P})^T$ upon which small amplitude perturbations $\mathbf{q}'(\mathbf{x},t) = (u',v',p')^T$ are permitted ($\mathbf{x} = (x,y)^T$). Normal mode solutions $\mathbf{q}'(\mathbf{x},t) = \hat{\mathbf{q}}(y)e^{i(kx-\omega t)}$ with $\hat{\mathbf{q}}(y) = (\hat{u},\hat{v},\hat{p})^T$ are then considered to model the spatial and temporal development of the perturbations. Note that k and ω are also nondimensionalized using the average velocity $\tilde{U}$ and the effective momentum thickness Θ_{eff}, defined and discussed in detail in Sec. IV A. The decomposed flow field is subsequently linearized by neglecting higher order perturbation terms. This yields a system of linear equations, which is solved as an eigenvalue problem (EVP) for the wave number $k = k_r + ik_i$ or for the frequency $\omega = \omega_r + i\omega_i$. Subscripts r and i stand for real and imaginary part, respectively.

The linear stability problem is considered in a finite domain in the streamwise direction, represented by the Kulikowskii condition, and in the wall-normal direction, characterized by the boundary conditions as depicted in Fig. 1. The free stream boundary conditions ($y = H$) of the EVP are of Neumann type for all three variables. In the cavity floor ($y = -H$) the boundary conditions for the velocities are of Dirichlet type due to the no-slip condition at the solid wall. The boundary condition for the pressure is of Neumann type, as follows from the momentum equation. The customary parallel flow assumptions $\overline{V} = 0$, $\overline{P} = \text{const}$ and $\partial_x\overline{Q} = 0$ are applied. The one-dimensional base state of the velocity field $\overline{U} = f(y)$ was nondimensionalized with the average velocity $\tilde{U}$ and the momentum thickness Θ_{eff}. It reads

$$\overline{U}(y) = 1 + \tanh\left(\tfrac{1}{2}y\right). \tag{3}$$

The EVP together with the base-flow assumptions yield the dispersion relation of the system, given by the complex equation

$$\Delta(\omega_r,\omega_i,k_r,k_i) = 0. \tag{4}$$

Its roots $\omega(k)$ provide the eigenfrequencies and growth rates. The dispersion relation is solved numerically using a Matlab code based on a Chebyshef collocation method with $N = 100$ collocation points in the wall-normal direction y. Differentiation is carried out using a second order nonequidistant finite difference method. According to the Rayleigh criterion, the inflexion point of the base profile is a necessary (yet not sufficient) condition for the base flow to be unstable to small perturbations. Whether instabilities occur and if so, whether they are are amplified or evanescent in space and time has to be determined by criteria described in Ref. [1]. It builds the basis for the LSAFD and will be shortly outlined in the next section.

A. Amplification and nontransparency

In order to present the argument that leads to the LSAFD, a brief outline of the steps needed to determine whether a medium, governed by its dispersion relation, amplifies or damps an infinitesimal perturbation is given. This theoretical consideration for the infinite domain is on one hand used to distinguish between upstream and downstream traveling waves (k_- and k_+, respectively) and, on the other hand, to study the asymptotic behavior of these waves. Normal mode properties, sustained by a given base state, are encapsulated in its dispersion relation (4). In general, both the wave number k and the frequency ω are considered complex. Solutions of the dispersion relation for given complex wave numbers are called temporal branches, whereas solutions of the dispersion relation for given complex frequencies are called spatial branches. The response of the system (the perturbation wave) to a source

$$g(x,t) = C\cdot\mathcal{H}(t)\delta(x)e^{-i\omega_0 t} \tag{5}$$

of a given frequency ω_0 is given by

$$\Psi(x,t) = \frac{C}{2\pi}\int_{L_\omega}\underbrace{\int_{F_k}\frac{e^{ikx}}{\Delta(\omega,k)}dk}_{\phi(\omega,x)}\frac{e^{-i\omega t}}{i(\omega-\omega_0)}d\omega, \tag{6}$$

where $\Delta(\omega,k)$ denotes the dispersion relation, $\mathcal{H}(t)$ the Heavyside step function in time, $\delta(x)$ the Dirac delta in space, and C a constant. The integration contours in the complex ω plane and the complex k plane, respectively, are defined according to $L_\omega = (-\infty + i\omega_i, +\infty + i\omega_i)$ where $\omega_i > 0$ and $F_k = (-\infty,+\infty)$. The integration contour L_ω is located above all the poles in the complex ω plane, as required by the

"causality principle," which states that "effect cannot precede cause," meaning that the perturbation occurs only after the source has been turned on at $t = 0$.

Below we discuss the asymptotic behavior of the response of the system perturbed with upstream and downstream traveling waves. To this end we consider the asymptotic behavior of expression (6).

B. Asymptotic behavior of the response of the system

In space, a perturbation can travel to $x < 0$ and to $x > 0$, whereas time is unidirectional and thus only $t > 0$ makes sense. Therefore, the sign of k cannot serve as an indicator of stability or instability, as in the temporal case. The physical nature of the behavior of the waves is embedded in its dispersion relation, which depends on the medium. In a transparent medium, the wave only possesses real parts of the frequency and the wave number. Thus, it passes without being affected by the medium. On the other hand, if the medium affects the wave it acquires an imaginary part, which accordingly yields an amplified or an evanescent wave. If the perturbation tends to zero as $x \to \pm\infty$ the wave is evanescent, while if the perturbation increases as $x \to \pm\infty$ the wave is amplified.

Following Ref. [1], we now look for the asymptotic form of the response of the system $\Psi(x,t)$, far from the source, i.e., for $|x| \to \infty$, and long after the time origin ($t \to \infty$). The asymptotic form $t \to \infty$ has to be taken before $|x| \to \infty$, as a perturbation cannot propagate to infinity in a finite amount of time. Applying Briggs' method [19] we consider Eq. (6) and move L_ω downwards (for a given $\omega_r = \omega_0$) in order to get the asymptotic expression in time. The highest located singularity in the complex ω plane is ω_0. Once this pole is reached, the asymptotic form of Eq. (6) reads

$$\Psi(x,t) \propto e^{-i\omega_0 t}\phi(\omega_0,x), \tag{7}$$

where only the second term $\phi(\omega_0,x)$ is of interest, since the first term simply oscillates. The poles of $\phi(\omega_0,x)$ are the zeros of the dispersion relation $\Delta(\omega_0,k)$ of the system. By definition, let $k_+(\omega)$ denote the poles located in the positive k half plane and $k_-(\omega)$ the poles located in the negative k half plane for $\omega_i \to \infty$. When the L_ω contour is lowered, the poles in the complex k plane move. They might stay in their original half plane or might cross into the other half plane. The poles of interest are the ones that are closest to the real k axis if they have not crossed, or the ones that are farthest from the real axis in the case they have crossed the k_r axis. With these values of k_+ and k_- the asymptotic behavior of the response of the system can be evaluated, considering

$$\begin{aligned}\Psi(x,t) &\propto e^{i[k_+(\omega_0)x-\omega_0 t]}\\ &= e^{i[k_{r+}(\omega_0)x-\omega_{r0}t]}e^{-k_{i+}(\omega_0)x+\omega_{0i}t}\end{aligned} \tag{8}$$

for $x > 0$ and

$$\begin{aligned}\Psi(x,t) &\propto e^{i[k_-(\omega_0)x-\omega_0 t]}\\ &= e^{i[k_{r-}(\omega_0)x-\omega_{r0}t]}e^{-k_{i-}(\omega_0)x+\omega_{0i}t}\end{aligned} \tag{9}$$

for $x < 0$. In the case studied in the present work, a k_+ branch crosses the k_r axis, while all k_- branches stay in the lower half plane. Thus, $k_{i+} < 0$ and $k_{i-} < 0$, which means that downstream traveling waves are amplified [Eq. (8)], while upstream traveling waves are evanescent [Eq. (9)]. This is commonly known as convective instability. Once the L_ω contour reaches the most unstable pole, a so-called branch point (BP) is formed. According to Ref. [20], it can be shown that when a BP occurs in the complex ω plane, a so-called pinch point (PP) occurs simultaneously in the complex k plane. Invoking the arguments introduced above, k_+ and k_- waves can be distinguished by considering their behavior for $\omega_i \to \infty$. A pole that moves to the positive half plane when $\omega \to \infty$ forms part of the k_+ family while a pole that moves to (or stays in) the negative half plane when $\omega \to \infty$ forms part of the k_- family.

III. THE FINITE DOMAIN

The finite extent of the domain becomes relevant when the times taken into consideration are larger than the time needed by the perturbation to travel along the cavity length. The geometry under consideration is characterized by its normalized length $L^* = \frac{L}{\Theta_{\text{eff}}}$, the cavity height $H^* = \frac{H}{\Theta_{\text{eff}}}$, and the two reflection coefficients R_2 and R_1 at the upstream and downstream boundaries, respectively. Θ_{eff} is the effective momentum thickness that is discussed in detail in Sec. IV A. L is of the same order as the wavelength of the perturbation and therefore cannot be neglected. The Kulikowskii condition is obtained, following Refs. [1] and [13]. Let P be an arbitrary point inside the domain emitting two countertraveling perturbation waves $k_+(\omega)$ and $k_-(\omega)$. Branches associated with $k_+(\omega)$ and $k_-(\omega)$ are found as solutions of the dispersion relation $\Delta(\omega,k)$ for complex wave numbers and complex frequencies in an infinite domain. As stated in Ref. [1], the characteristic oscillations of a finite system may be regarded as the result of the superposition of traveling waves reflected by the two boundaries, represented by R_1 and $R_2 \in \mathbb{R}$. The reflections are accompanied by a mutual transformation of waves belonging to different branches of the spectrum. Formally the Kulikowskii condition is obtained by considering the perturbation wave

$$\Psi(x,t) = A_0 e^{i[k_+(\omega)x-\omega t]}, \tag{10}$$

which is emitted at P $(0 < P < L^*)$. A_0 is the initially infinitesimal amplitude. When it reaches the downstream boundary, Ψ is reflected according to reflection coefficient R_1, and sent back upstream. The wave on its way upstream is described by

$$\Psi(x,t) = R_1 A_0 e^{ik_+(\omega)L^*} e^{i[k_-(\omega)(x-L^*)-\omega t]}. \tag{11}$$

It reaches the upstream boundary, where it is reflected again, according to the reflection coefficient R_2. When it travels downstream again the wave is described by

$$\Psi(x,t) = R_1 R_2 A_0 e^{i[k_+(\omega)-k_-(\omega)]L^*} e^{i[k_+(\omega)x-\omega t]}. \tag{12}$$

Due to the requirement that $\Psi(x,t)$ must be single valued, Eqs. (10) and (12) must coincide, leading to the Kulikowskii condition

$$R_1 R_2 e^{[i(k_+-k_-)L^*]} = 1. \tag{13}$$

Note that the frequencies for the downstream traveling waves (10) and the upstream traveling wave (11) and (12) do not change. Hence the frequencies of the $k_+(\omega)$ and $k_-(\omega)$

TABLE I. Summary of $L/H = 2$ cavity cases. Free stream velocity, U_∞. Momentum thickness of boundary layer at $x = 0$, Θ_0. Cavity length, L. Location of best fit, $x_{\min}$. Effective momentum thickness, Θ_{eff}. Normalized cavity height, $H^*_{\text{eff}} = \frac{H}{\Theta_{\text{eff}}}$. Selected Kulikowskii modes, m_1 and m_2.

Case	Symbols	$U_\infty(\frac{\text{m}}{\text{s}})$	Θ_0 (mm)	L (mm)	$x_{\min}/L(-)$	Θ_{eff} (mm)	$H^*_{\text{eff}}(-)$	m_1	m_2
LH20	•	2.250	—	100	—	1.296[a]	38.6	3	8
LH21	○	2.180	1.072	100	0.227	1.325	37.7	4	8
LH22	△	1.898	1.294	100	0.227	1.425	35.1	4	8
LH23	▽	1.715	1.260	100	0.250	1.525	32.8	5	9
LH24	□	1.379	1.310	100	0.227	1.675	29.9	5	–
LH25	▲	0.992	1.420	100	0.250	1.975	25.3	5	–

[a]Momentum thickness was not obtained experimentally but extrapolated from cases LH21 to LH25.

waves are the same. The Kulikowskii condition is a complex equation which can be split up into a real and an imaginary part. This yields

$$\Delta k_r = k_{r+}(\omega) - k_{r-}(\omega) = \frac{\pi \text{m}}{L^*}, \tag{14}$$

$$\Delta k_i = k_{i-}(\omega) - k_{i+}(\omega) = \frac{1}{L^*} \ln\left[\frac{1}{R_1 R_2}\right] \approx 0, \tag{15}$$

where $\text{m} \in \mathbb{N}_0$. Poles of the linear stability analysis which also solve Eqs. (14) and (15) will hereafter be called *Kulikowskii points*.

A. Reflection coefficients

As we consider a rigid cavity walls, the reflection coefficients are assumed to be real with a phase shift of π. Following Ref. [14] we impose a zero total deformation boundary condition at the upstream and downstream corner of the cavity, which is expressed as

$$\Psi(x = 0,t) = 0, \tag{16}$$

$$\Psi(x = L,t) = 0. \tag{17}$$

Let us denote A_1^+ the amplitude of the wave at the downstream boundary (1) before it was reflected and let us denote A_1^- the amplitude of the wave at the downstream boundary (1) after it was reflected. Then we can write the deformation $\Psi(x = 0,t)$ at the location where the boundary condition is imposed as the sum of the two waves k_+ and k_-, which have to add up to zero. This yields (for all times t)

$$\Psi(x = 0,t) = [A_2^+ e^{ik_+ x} + A_2^- R_1 e^{ik_- x}]e^{-i\omega t} = 0, \tag{18}$$

$$\Psi(x = 0,t) = A_2^+ + A_2^- R_1 = 0, \tag{19}$$

$$R_1 = -\frac{A_2^+}{A_2^-} = -1 \tag{20}$$

if we assume that no forcing is induced by the boundaries and therefore the amplitudes before and after the reflection are the same. The same reasoning holds for the upstream boundary (2) from which follows $R_2 = -1$.

Physically it is plausible to expect the product of the reflection coefficients to be smaller than unity since a part of the perturbation wave could be lost and travel off to infinity. A rough computation following Lighthill [21] gave a value of $R_1 R_2 \approx 0.8$ which translates into $\Delta k_i = 0.0029$ for case LH21 (see Table I) when applied to Eq. (15). The effect of this positive difference of the spatial amplification rates is depicted in Fig. 2. Since the real part of the frequency does not change upon reflection, the Kulikowskii points for $\Delta k_i = 0$ (red ▽) must move on branches $\omega_r = \text{const}$ (indicated by black circles in Fig. 2) until the corresponding Δk_i is reached. The resulting difference in the real part of the wave number Δk_r is approximately equal to Δk_r for $R_1 R_2 = 1$. This is true even for values $R_1 R_2 < 0.8$ since the branches $\omega_r = \text{const}$ are predominantly vertical and therefore Δk_r changes only little when Δk_i is increased.

Based on the considerations outlined above we propose a first order approximation, assuming the reflection coefficients to be $R_1 = R_2 = -1$.

B. Interpretation of the Kulikowskii condition

Physically, Eq. (14) states that the finite domain can contain only an integer number of waves, which is in agreement with the wavelength selection criterion found in Ref. [22]. This

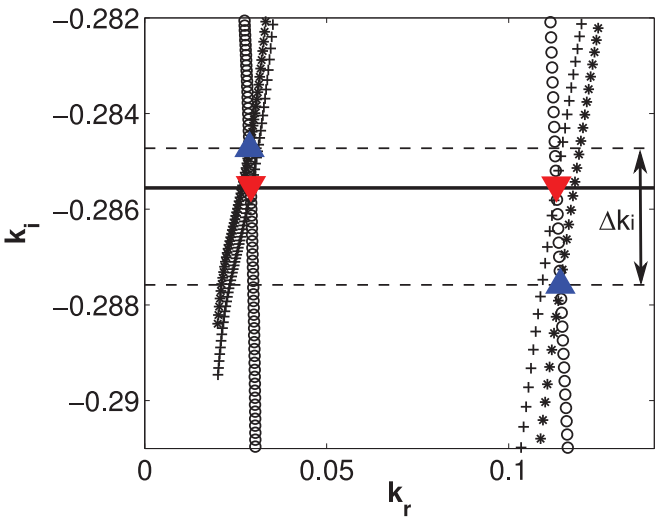

FIG. 2. (Color online) LSAFD with $\Delta ki = 0.0029$, which translates into $R_1 R_2 = 0.80$. Case LH21: Branches (+) and branches (•) correspond to different $\omega_i = \text{const}$; Branches (○) correspond to $\omega_r = \text{const}$. Horizontal solid line indicates $\Delta ki = 0$ ($R_1 R_2 = 1$) for Kulikowskii points (red ▽). Horizontal dashed lines separate Kulikowksii points (blue △) by $\Delta k_i = 0.0029$ ($R_1 R_2 = 0.8$).

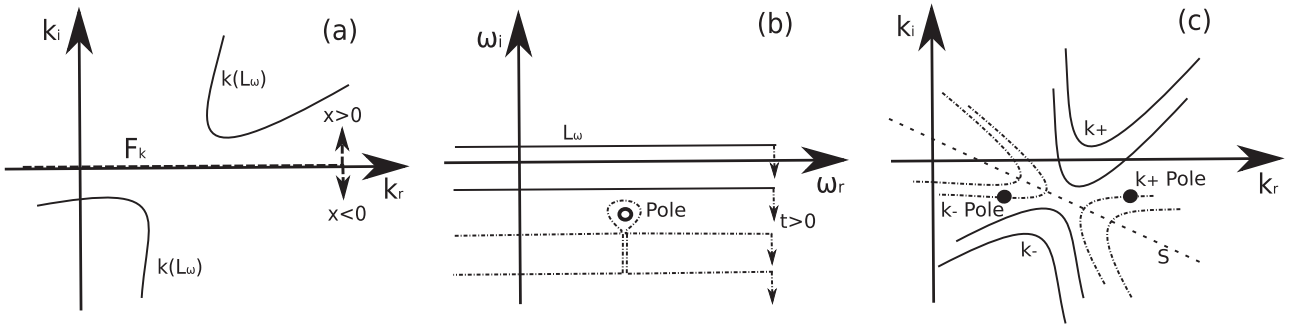

FIG. 3. (a) Complex k plane with k branches for $\omega_i \to \infty$. (b) Complex ω plane with integration contours before (——) and after (– · –) the branch point is crossed. (c) k branches before (——) and after (– · –) the branch point is crossed, together with two exemplary poles (•) that solve the Kulikowskii Condition. The straight dashed line S (– – –), separates k_+ poles from k_- poles. The dashed arrows indicate movement of respective poles when $\omega_i \to \infty$.

yields a discretization of a continuous spectrum of solutions and thus will lead to a selection mechanism of the associated frequency. Note that in the infinite domain ($L \to \infty$) such a discretization does not occur since $\Delta k_r = 0 \ \forall m \in \mathbb{N}$. The second equation (15) states the coincidence condition in terms of the spatial growth rates. The difference of the spatial growth rates for the upstream and downstream traveling waves has to be compensated by the reflection coefficients R_1 and R_2, to prevent the system from getting out of balance. Hence, Eq. (15) expresses the self-limited nature of the system. For the case of total reflection, the right-hand side of Eq. (15) is zero, which means that if the amplitude of the perturbation wave is not diminished by reflection, the spatial amplification rates of the upstream and downstream traveling waves must be equal in absolute terms. The more general case of $R_1 R_2 \neq 1$ yields a strictly positive right-hand side of Eq. (15) and the amplification rates adapt accordingly in order to maintain valid Eq. (15). However, since as mentioned above the product of the reflection coefficients is close to unity, the numerical value of Δk_i is small and does not affect the results significantly.

In short, the solutions to the Kulikowskii condition consist of two different values of k_r, which are associated with one single set of values of k_i, ω_r, and ω_i. Poles of the linear stability analysis in the infinite domain that also solve the finite domain constraint, namely, the Kulikowskii condition, are denoted Kulikowskii points. Kulikowskii points therefore characterize the instability behavior of the finite system.

C. Evaluation of the Kulikowskii condition

As stated above, the right-hand side of Eq. (15) is always positive or zero, since $0 \leqslant R_1 R_2 \leqslant 1$. For the conventional case (i.e., $\omega_i > \omega_{i\mathrm{BP}}$), however, the respective locations of the k_+ branch and the k_- branch [see Fig. 3(a)] do not allow for such a solution, since the k_+ branch is located above the k_- branch, which will always yield $k_-(\omega) - k_+(\omega) \leqslant 0$. The only point where the equation holds is the PP itself. However, if the BP is crossed (i.e., $\omega_i < \omega_{i\mathrm{BP}}$) by means of analytic continuation of the L_ω contour, as depicted in Fig. 3(b), the branches change their location so that nonzero solutions for Eq. (15) become possible. As stated in Sec. II A, once the integration contour L_ω crosses the least stable pole in the ω plane, causality is violated. This holds for the infinite domain in which the reflection of the perturbation wave is not taken into account. In the case of a finite domain, the concepts of "before" and "after" become inadequate, since due to reflection, a wave has to be considered as cause and effect at the same time. In order to know whether a pole is located on a k_+ branch or a k_- branch, the same criterion as before is applied. A pole that moves to the upper half plane as $\omega_i \to \infty$ is located on a k_+ branch, while a pole that stays in the lower half plane when $\omega_i \to \infty$, is located on a k_- branch. The straight dashed line in Fig. 3(c) separates the two types of branches according to this criterion.

IV. RESULTS

A. Experiments and momentum thickness

The results of the LSAFD are now compared to experimental results obtained by Refs. [11] and [12]. The momentum thickness Θ is the only variable parameter in the analysis. As noted in Ref. [23] (and confirmed in the present work), the analysis is quite sensitive to Θ. It is therefore crucial to choose the momentum thickness with care. The base profile is assumed to follow the shape of a hyperbolic tangent function. Hence, the incoming Blasius boundary layer needs a certain time (and space) to relax, in order to fit the hyperbolic tangent assumption. The authors of Ref. [24] propose to choose Θ in the vicinity of the plateau where the momentum thickness varies only marginally, i.e., $\frac{\partial \Theta}{\partial x} \approx 0$. Since the plateau in our case is found at approximately $0.1 < x/L < 0.45$, the base profile [Eq. (3)] was fitted in this region to the experimental velocity profiles [12] along the cavity length with a least-square fit method as done by Ref. [25] and Θ was taken at the streamwise position $x_{\min}$, for which the least-square error $(U_{\tan} - U_{\exp})^2$ exhibits a minimum. $x_{\min}$ was found to be at approximately one quarter of the cavity length. This is in agreement with Ref. [23], which suggests using the value of Θ one instability wave length downstream of the trailing edge and before any significant nonlinear interactions occur. Thus instead of the inflow momentum thickness Θ_0, an effective momentum thickness $\Theta_{\mathrm{eff}} = \Theta(x_{\min})$ is used as length scale.

Table I summarizes the six cases analyzed in the present work. The cavity geometry (L/H) is kept constant and only the free stream velocity U_∞ is varied. With U_∞ changes Θ_0 and

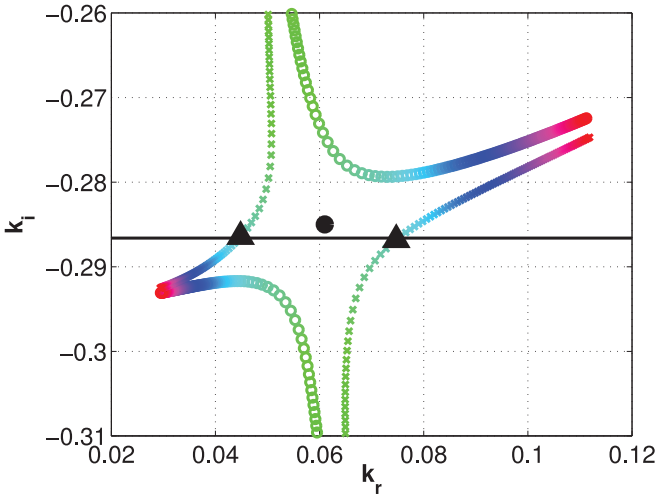

FIG. 4. (Color online) k branches in complex k plane for $\omega_i = -0.0632$ (○) and $\omega_i = -0.0636$ (×) for case LH21. Color scale indicates value of increasing ω_r from light green ($\omega_r = 0.1676$) to red ($\omega_r = 0.1728$). Pinch point marked by ●. Kulikowskii points marked by ▲. Horizontal solid line (—) indicates $k_i = \text{const}$.

therefore Θ_{eff}, which likewise affects the normalized cavity height and length, H^* and L^*, respectively.

B. Evaluation of the Kulikowskii condition

Figure 4 shows four branches, that result from mapping $\omega_i = \text{const}$ through the dispersion relation into the complex k plane, before (circles) and after (crosses) the branch point is crossed. Comparison between the (○) branch and the (+) branch shows that, as stated above, solutions of the Kulikowskii condition [Eqs. (14) and (15)] are possible only after the BP is reached. Solutions to the Kulikowskii condition are called Kulikowskii points. The mapping of a Kulikowskii point from the k plane into the ω plane is depicted in Fig. 5. By means of a spatial analysis $k_i = \text{const}$ is mapped through the

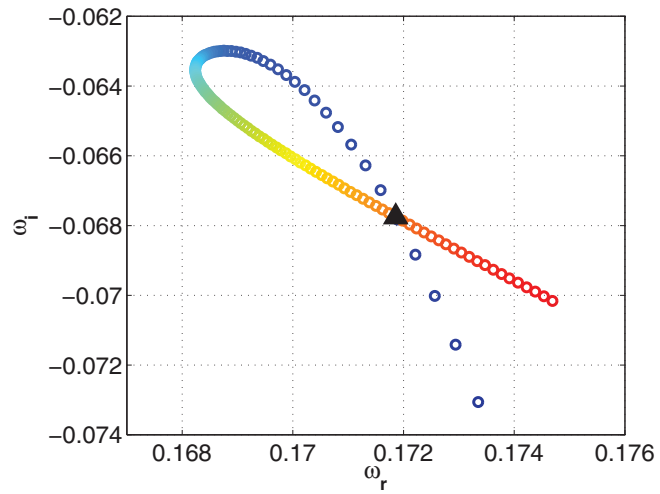

FIG. 5. (Color online) ω branch for $k_i = -0.3015$. Intersection (▲) indicates Kulikowskii point. Color scale indicates value of increasing k_r from blue ($k_r = 0.0220$) to red ($k_r = 0.1400$).

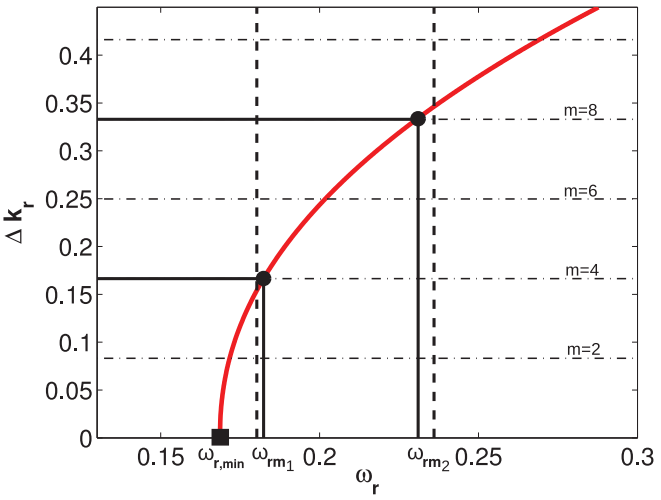

FIG. 6. (Color online) Red solid graph (—) shows continuous set of solutions to Eq. (15). Horizontal lines (– · –) depict solutions to Eq. (14) for $m = 2, \ldots, 10$. Vertical solid lines (—) indicate by the LSAFD selected frequencies ω_{rm_1} and ω_{rm_2}. Dashed vertical lines (– – –) indicate frequencies obtained experimentally [11,12]. The pinch point is marked by ■ and indicates the minimum frequency $\omega_{r,\min}$ selected by the LSAFD. Kulikowskii points are marked by ●. Only case LH21 is depicted for the sake of clarity.

dispersion relation into the complex ω plane and results in a self-intersecting branch. The intersection yields a Kulikowskii point as the following conditions are met:

$$\omega_{i+} = \omega_{i-}, \tag{21}$$

$$\omega_{r+} = \omega_{r-}, \tag{22}$$

$$k_{i+} = k_{i-}, \tag{23}$$

$$k_{r+} = k_{r-} + \frac{\pi \mathrm{m}}{L^*} \qquad \mathrm{m} \in \mathbb{N}_0. \tag{24}$$

A special solution to the Kulkowskii condition is obtained for $\mathrm{m} = 0$. This double root of the dispersion relation is commonly called a *pinch point* in the literature. Evaluating the second Kulikowskii condition [Eq. (15)] results in the continuous red graph in Fig. 6. For various $k_i = \text{const}$, $\Delta k_r(\omega_r) = k_{r+}(\omega_r) - k_{r-}(\omega_r)$ is plotted over the associated frequency ω_r. The quadratic form confirms the validity of the Taylor series expansion of the dispersion relation around the pinch point [1], which yields $k - k_0 \sim \pm(\omega - \omega_0)^{\frac{1}{2}}$. The continuous spectrum obtained by the second Kulikowskii condition is discretized by the right-hand side of the first Kulikowskii condition [Eq. (14)], which adds the horizontal lines to Fig. 6 and thus selects a set of discrete frequencies ω_{rm}, $\mathrm{m} \in \mathbb{N}_0$. Certain frequencies, labeled ω_{rm_1} and ω_{rm_2}, compare well with experimental results [11,12] shown in Fig. 7.

Figure 7 compares experimental results for the open-cavity flow [11,12] with the results of the LSAFD. The square root of the power spectral density (PSD), normalized by the respective maximum value, is depicted as a function of the free stream velocity U_∞ and the frequency f. The cases investigated

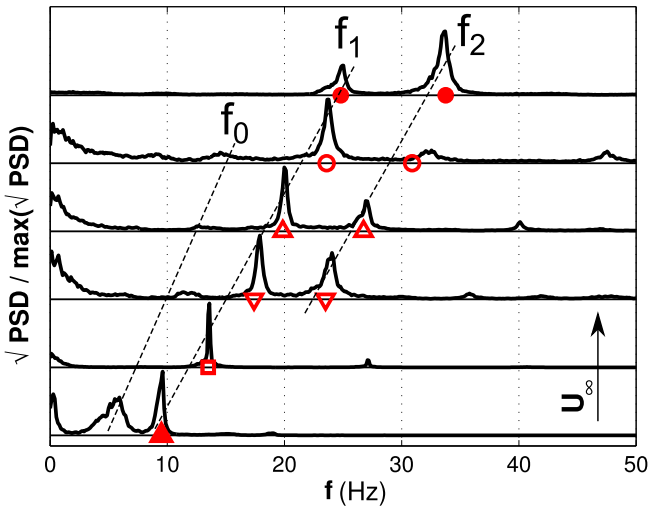

FIG. 7. (Color online) Y offset graph comparing the results from LSAFD (red symbols as in Table I) with the square root of the normalized power spectral density (PSD) of experimental results [11,12] (black graphs), measured using an LDV technique. The streamwise velocity component for the six cases in Table I is depicted. Dashed lines indicate frequency branches f_0, f_1, and f_2. The arrow indicates the direction of increasing U_∞.

in the present work are represented by the thick lines and U_∞ varies in the vertical axis as indicated by the arrow. Results of the LSAFD are indicated by the red symbols. Three incommensurable frequency branches (denoted f_0, f_1, f_2 in the graph) are amplified depending on U_∞. At low velocities f_0 and f_1 coexist, though f_0 is dominant. While f_0 disappears for velocities larger than $U_\infty \approx 1.4$, f_1 keeps growing until it dies out for velocities $U_\infty > 2.5$. f_2 starts to develop around $U_\infty \approx 1.6$ and keeps growing from there on. f_0 lies outside of the frequency range selected by the Kulikowskii condition and is therefore assumed to be due to other effects, mentioned in the introduction [6,8]. The two high-frequency branches f_1 and f_2 enter the regime predicted by the LSAFD for all velocities.

Frequencies selected by the Kulikowskii condition for $m = 4,5$ and $m = 8,9$, respectively, are in good agreement with experimental data [11,12]. However, the Kulikowskii condition selects a larger number of discrete frequencies than experimentally observed.

C. Evolution of Kulikowskii modes in space and time

The values of k_i and ω_i along the Kulikowskii points are depicted in Figs. 8 and 9, respectively. In accordance with Eqs. (8) and (9), a negative value of k_i amplifies downstream traveling waves and attenuates upstream traveling waves as required by the Kulikowskii condition. Close to the cutoff frequency $\omega_{r,\min}$ (which is nearly equal for all six cases), the value of k_i changes rapidly, whereas the increase or decrease depends on the local topology of the PP. Farther away from $\omega_{r,\min}$ the value of k_i levels out and tends to a constant, hence being approximately equal for both amplified frequencies ω_{rm_1} and ω_{rm_2}.

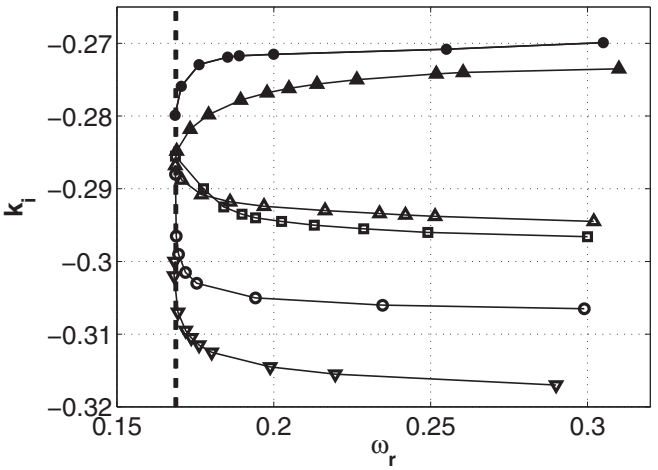

FIG. 8. Values of k_i for different cases.

The value of ω_i is negative throughout the entire frequency band. This is in accordance with the convective nature of the instabilities in the present flow and the idea of spatially amplified waves. If ω_i were positive, the perturbations would grow exponentially in time in every point in space and thus contaminate the entire flow (absolute instability). The value of ω_i as a function of ω_r drops linearly (with slope ≈ -1) moving away from the cutoff frequency. This means that mode m_2 is temporally more damped than mode m_1. A mechanism which eludes the predominance of either one of the modes, as discussed in Ref. [26], could not be identified by the present theory. However, it should be noticed that the temporal growth rate has only a weak meaning in the present work since we do not consider an infinitely extended shear layer, but a system confined by boundaries within which the question of self-sustaining modes induced by the constructive interference of reflected waves is addressed.

D. Eigenfunctions of Kulikowskii modes

The location of Kulikowskii points in their respective complex planes yields information on the stability behavior as

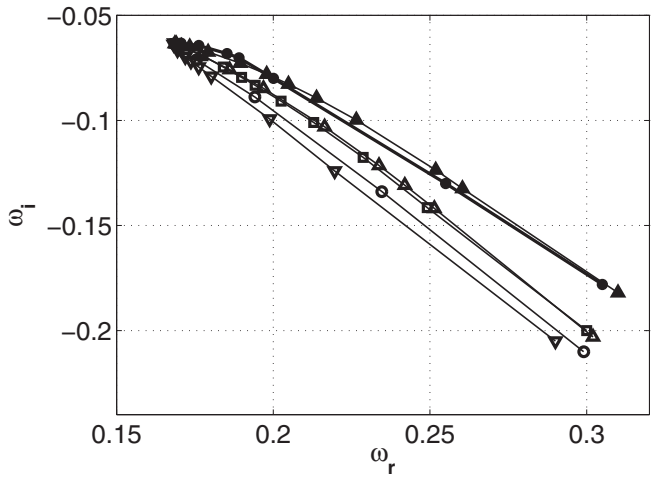

FIG. 9. Values of ω_i for different cases. Symbols as in Table I.

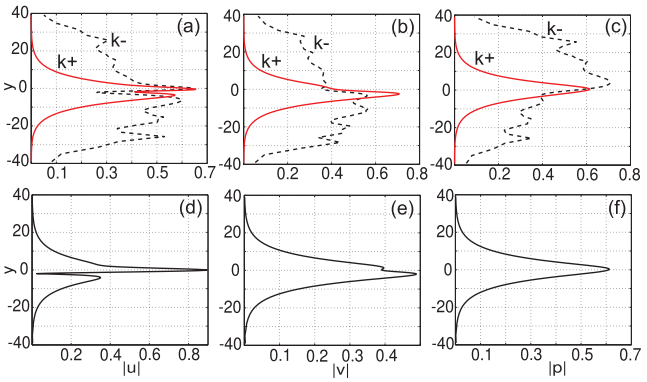

FIG. 10. (Color online) (a–c) Eigenmodes of amplifying k_+ waves (solid lines) and evanescent k_- waves (dashed lines) of $m = m_1$ of case LH21 ($\omega_r = 0.1848$, $\omega_i = -0.0801$). (d–f) Kelvin-Helmholtz modes of same frequency $\omega_r = 0.1848$, but $\omega_i = 0$.

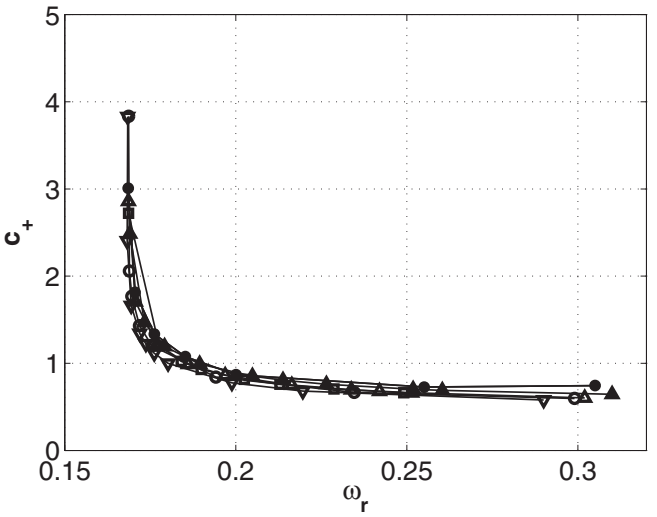

FIG. 11. Phase speeds of k_+ waves for all cases.

well as on the wave number and frequency of the perturbation waves. The corresponding eigenfunctions provide further information on the structure of the respective waves in their three components u, v, and p. Figures 10(a)–10(c) shows the eigenmodes for the streamwise velocity perturbation u, wall-normal velocity perturbation v, and pressure perturbation p of a single set of Kulikowskii points (k_+ and k_-) at approximately the frequency corresponding to mode m_1 ($\omega_r = 0.1848$) of case LH21. For the same frequency, Figs. 10(d)–10(f) shows the u, v, and p eigenmodes corresponding to the pole on the Kelvin-Helmholtz (KH) branch. Comparing the k_+ perturbations structure with the KH perturbation structure it becomes clear that the amplifying k_+ wave is a KH-like perturbation. This is in accordance with the general picture of the cavity mechanism. The components of the evanescent k_- wave [dashed lines in Figs. 10(a)–10(c)] do not resemble the KH modes. In all three components their amplitudes show a more dispersed behavior. The velocity components of the k_- modes are most active inside the cavity ($y < 0$), while the pressure component shows a maximum above the cavity ($y > 0$). Which one of the components is responsible for the reflection mechanism cannot be clearly identified; however, it can be stated that while the downstream traveling k_+ waves are active in a rather narrow region close to the center line ($y = 0$), the upstream traveling k_- waves are active over the entire domain ($-H < y < H$). It is worthwhile noting that the choice of the KH like k_+ branch is not arbitrary but follows directly from the spatiotemporal stability theory described in Sec. II, which states that the k_+ branch to be chosen is the one with the greatest negative value of k_{i+} [1]. The choice of the k_- branch is dictated by the Kulikowskii condition.

E. Phase speed of Kulikowskii modes

Figures 11 and 12 show the phase speed of the downstream traveling k_+ waves and the upstream traveling k_- waves, respectively, as a function of the frequency for the six cases summarized in Table I. The dimensionless phase speed of the downstream and upstream traveling waves, respectively, is defined as

$$c_\pm = \frac{\omega}{k_\pm}. \tag{25}$$

As shown in Fig. 11, c_+ increases near the pinch point singularity but tends to a constant value of approximately $c_+ \approx 0.6$ for larger frequencies. All six cases collapse in a single line. Figure 12 depicts the phase speed of the upstream traveling waves for the different cases together with the nondimensional speed of sound in air

$$a = \frac{a_\infty}{U_\infty} \quad \text{with} \quad a_\infty = 340\,\text{m/s}. \tag{26}$$

For the feedback mechanism to be acoustic, waves must travel at the speed of sound. As shown in Fig. 12 the upstream traveling waves travel in fact substantially faster than the downstream traveling waves, but do still not reach the speed of sound in the frequency band where the amplified

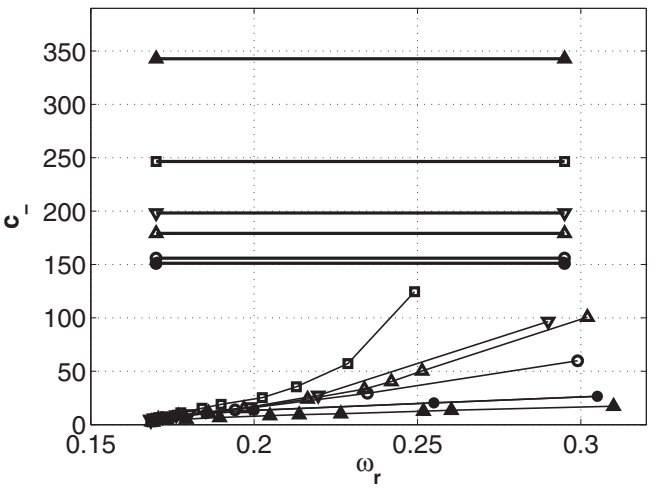

FIG. 12. Phase speeds of k_- waves. Symbols as in Table I. Dashed horizontal lines indicate nondimensionalized speed of sound in air $a^* = \frac{a_\infty}{U_\infty}$ of the respective case.

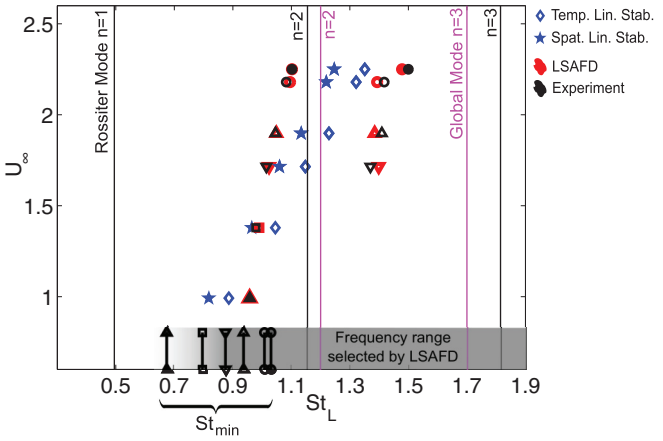

FIG. 13. (Color online) Comparison of experimental results [11,12] (black) with LSAFD (red) for all six cases as well as with a temporal (spatial) linear stability in infinite domain marked by blue ◊ (⋆). Long vertical black lines show Rossiter modes $n = 1,2,3$ from Eq. (27). Long vertical magenda lines show global modes $n = 2,3$ from Ref. [10]. Short vertical lines show minimum Strouhal number $St_{\min} = \frac{\omega_{r,\min} L^*}{4\pi}$, defined by pinch point frequency of the respective cases (see Fig. 6). Gray shaded area shows frequency range selected by LSAFD ($St > St_{\min}$). Symbols as in Table I.

frequencies are observed experimentally ($0.18 < \omega_r < 0.27$). These results suggest that the feedback mechanism in the incompressible limit is rather due to slower traveling instability waves than to acoustic pressure waves.

F. Discussion

Figure 13 compares the results obtained by the LSAFD with data from several other works in the literature. Results from the LSAFD ($St_{L,\mathrm{FD}} = \frac{\omega L^*}{4\pi}$, red symbols) compare well with experimental results [12] ($St_{L,\exp} = \frac{f_{\exp} L}{U_\infty}$, black symbols). The blue diamond ◊ (or star ⋆) symbols in Fig. 13 show the Strouhal number $St_{L,\mathrm{LS}} = \frac{\omega_{\mathrm{LS}} L^*}{4\pi}$ of a conventional local temporal (or spatial) linear stability analysis in an infinite domain (i.e., no Kulikowskii condition applied), where $\omega_{\mathrm{LS}}(k_r)$ is the frequency for which $\omega_i(k_r)$ [or $k_i(\omega_r)$] is maximal (or minimal). The conventional (temporal or spatial) linear stability analysis can, however, predict only one single amplified frequency which tends to fall between the two nonharmonic peaks observed experimentally and does not predict either one of them with clarity.

As mentioned in the introduction, high subsonic compressible open-cavity flow is commonly related to the acoustic feedback mechanism (*Rossiter mechanism*) expressed in terms of the Strouhal number $St_{L,R}$ by the semiempirical Rossiter [7] formula

$$St_{L,R} = \frac{f_R L}{U_\infty} = \frac{n-\gamma}{M + \frac{1}{\kappa}}, \tag{27}$$

which was derived under the assumption that the feedback waves travel upstream at the speed $c = \frac{\omega}{k}$ where c is the speed of sound c. In the incompressible limit the Mach number is zero and the cavity length L is given in Table I. In Eq. (27) $n = 1,2,3\ldots$ is the mode number, κ is the ratio between the convection speed of the vortices and the free stream velocity, and γ is the lag time between the impact of a vortex on the cavity edge and the emission of an acoustic wave. The values $\kappa = 0.66$ and $\gamma = 0.25$ were used [9]. As mentioned by Ref. [5] for the $L/H = 2$ cavity the first two Rossiter modes are prevalent in the compressible case. Reference [10] tried to link the Rossiter mechanism to the results of a global instability analysis when approaching the incompressible limit. However, only for mode $n = 2$ could a good agreement be found. In Fig. 13 Rossiter's results for $M = 0$ (vertical lines) are compared with the global linear stability results [10], with the results from the LSAFD (red symbols), the results from a spatial linear stability analysis (blue stars), the results from a temporal linear stability analysis (blue diamonds), and the experimental results [11,12] (black symbols) for the six cases evaluated in the present work (see Table I).

Rossiter mode 1 does not enter the frequency range selected by the LSAFD (gray shaded area in Fig. 13), given by the cutoff Strouhal number $St_{\min}$, which is defined by the pinch point frequency $\omega_{r,\min}$ in Fig. 6. This is in agreement with Ref. [10], which found Rossiter's mode 1 to be absent when approaching $M = 0$. Frequencies smaller than $St_{\min}$ are outside of the selectable frequency range, while the frequency band above $St_{L,\min}$ is discretized by the finite extent of the domain. Experimentally obtained frequencies [11,12] can be found at $St > St_{\min}$. Rossiter modes for $n = 2$ and $n = 3$ are also found within the discretized frequency band; however, they do not compare well with experimental results by Refs. [11] and [12]. Rossiter's mode 2 is somewhat close to the experimental mode 1, but Rossiter's mode 3 is found at substantially higher frequencies than the experimental mode 2. Global modes [10] compare reasonably well to Rossiter's modes but neither to the experimental results nor to the results obtained by the LSAFD.

These results indicate that in the incompressible limit the mechanisms responsible for the existence of nonharmonic modes are at least partly due to the reflection and the linear interaction of instabilities in the shear layer. This mechanism is not included in the acoustic feedback mechanism of Rossiter's formula.

V. CONCLUSIONS

This work reports results obtained by combining a local, incompressible linear stability analysis in the infinite domain with the so-called Kulikowskii condition, first introduced by Kulikowskii [13] and later revisited by Landau and Lifshitz [1], which limits the streamwise coordinate to L and takes into account the reflection of the perturbation waves. A theoretical framework for a linear stability analysis in a finite streamwise direction was developed. A wave reflection scenario was introduced in which downstream traveling k_+ waves are reflected into upstream traveling k_- waves and vice versa at the respective boundary. Total reflection was assumed, though the implications and consequences of nontotal reflection were outlined. As a result the Kulikowskii condition discretizes the frequency band in which the amplified nonharmonic frequencies are observed experimentally. It was found that the downstream traveling k_+ waves are spatially amplified and temporally damped, while the upstream traveling k_- waves are spatially and temporally attenuated. This results in a convective

type of instability, a necessary condition for Kulikowskii's theory to be applicable. Solutions to the Kulikowskii condition become possible only after the pinch point singularity is crossed, which yields a minimum frequency $\omega_{r,\min}$ (or $St_{\Theta,\min}$, respectively) that can be selected by the LSAFD.

The momentum thickness of the base profile used in the local linear stability analysis was chosen by a least square fit to experimental data [11,12] in accordance with previous works [23–25]. Kulikowskii's condition was evaluated for six different free stream velocities in a $L/H = 2$ cavity, yielding discrete frequencies ω_{rm_1} and ω_{rm_2}, respectively, that compare well with experiments [11]. It was found that the finite extent of the geometry is a necessary condition for the discretization of the frequency band. The low frequency content of the spectrum of the experimental data [11,12] f_0 (Fig. 7) was found to lie outside of the predicted regime ($\omega > \omega_{r,\min}$). It is concluded that another mechanism [6,8] must be at play than for the higher frequencies peaks f_1 and f_2 which enter the predicted regime and compare well with experimental results [11,12]. The frequency of mode 1 predicted by Rossiter's semiempirical formula [Eq. (27)], which is based on an compressible assumption, is also found outside of the regime ($St < St_{\Theta,\min}$). Frequencies of Rossiter's mode 2 and 3 enter the predicted regime, which is in agreement with Ref. [10]. However, the results of Ref. [10] do not compare well with experimental data in Refs. [11] and [12].

Our results indicate that the rather simple linear wave interaction model which is based on a local linear stability analysis and Kulikowskii's condition, describes well the nonharmonic modes observed experimentally. Thus in the incompressible limit the mechanisms responsible for the existence of nonharmonic modes are at least partly due to the reflection and the linear interaction of instabilities in the shear layer. This mechanism is not included in the acoustic feedback mechanism of Rossiter's formula. In our model the upstream traveling k_- waves are found to travel substantially faster than the downstream traveling k_+ waves, though do not reach the speed of sound.

ACKNOWLEDGMENTS

We wish to acknowledge the support by the CONICET under Grant No. 3303, UBACYT under Grant No. 100228, Science-Accueil d'Université Paris-Sud, LIA-PMF/FMF, and the 13STIC-08-P-MVP project of the StiCAmSud program. F.T. greatly acknowledges support of his PhD thesis by CONICET, Erich-Becker-Studienstiftung, and the DAAD.

[1] L. D. Landau and E. M. Lifshitz, *Physical Kinetics* (Robert Maxwell, Moscow, 1985), pp. 281–283.
[2] P. Huerre and P. Monkewitz, J. Fluid Mech. **159**, 151 (1985).
[3] A. Michalke, J. Fluid Mech. **19**, 543 (1964).
[4] J. Basley, Ph.D. thesis, Université Paris Sud & Monash University, 2012.
[5] C. W. Rowley, T. Colonius, and A. J. Basuz, J. Fluid Mech. **455**, 315 (2002).
[6] G. Bres and T. Colonius, J. Fluid Mech. **599**, 309 (2008).
[7] J. Rossiter, Internal Report, Ministry of Aviation (USA) **3438** (1964).
[8] E. Villermaux and E. Hopfinger, Physica D **72**, 230 (1994).
[9] N. Delprat, Phys. Fluids **18**, 071703 (2006).
[10] S. Yamouni, D. Sipp, and L. Jacquin, J. Fluid Mech. **717**, 134 (2013).
[11] F. Lusseyran, L. Pastur, and C. Letellier, Phys. Fluids **20**, 114101 (2008).
[12] J. Basley, L. Pastur, F. Lusseyran, T. Faure, and N. Delprat, Exp. Fluids **50**, 905 (2010).
[13] A. Kulikowskii, J. Appl. Math. Mech. **30**, 180 (1966).
[14] O. Doare and E. de Langre, Eur. J. Mech. B **25**, 948 (2006).
[15] F. Gallaire and J.-M. Chomaz, Phys. Fluids **16**, 274 (2004).
[16] R. S. Lindzen and A. J. Rosenthal, J. Atmos. Sci. **40**, 530 (1983).
[17] A. Kulikowskii, J. Appl. Math. Mech. **70**, 229 (2006).
[18] V. Theofilis, Annu. Rev. Fluid Mech. **43**, 319 (2011).
[19] R. Briggs, *Electron-Stream Interaction with Plasmas* (MIT Press, Cambridge, MA, 1964).
[20] P. J. Schmid and D. S. Henningson, *Stability and Transition in Shear Flows*, Applied Mathematical Sciences Vol. 142 (Springer, Berlin, 2001).
[21] J. Lighthill, *Waves in Fluids* (Cambrdige University Press, Cambrdige, UK, 1990), p. 100.
[22] A. Maurel, P. Ern, B. J. A. Zielinska, and J. E. Wesfreid, Phys. Rev. E **54**, 3643 (1996).
[23] C. Ho and P. Huerre, Ann. Rev. Fluid. Mech. **16**, 365 (1984).
[24] D. Hammond and L. Redekopp, J. Fluid Mech. **331**, 231 (1997).
[25] C. Tam and P. Block, J. Fluid Mech. **89**, 373 (1987).
[26] L. R. Pastur, F. Lusseyran, T. M. Faure, Y. Fraigneau, R. Pethieu, and P. Debesse, Exp. Fluids **44**, 597 (2008).